This is a repository copy of *Investigation of a novel AlZnN semiconductor alloy*.

White Rose Research Online URL for this paper:
http://eprints.whiterose.ac.uk/164071/

Version: Published Version

**Article:**

Trapalis, A. orcid.org/0000-0003-4887-7058, Fry, P.W., Kennedy, K. et al. (4 more authors) (2020) Investigation of a novel AlZnN semiconductor alloy. Materials Letters: X, 7. 100052. ISSN 2590-1508

https://doi.org/10.1016/j.mlblux.2020.100052

**Reuse**
This article is distributed under the terms of the Creative Commons Attribution (CC BY) licence. This licence allows you to distribute, remix, tweak, and build upon the work, even commercially, as long as you credit the authors for the original work. More information and the full terms of the licence here:
https://creativecommons.org/licenses/

**Takedown**
If you consider content in White Rose Research Online to be in breach of UK law, please notify us by emailing eprints@whiterose.ac.uk including the URL of the record and the reason for the withdrawal request.

eprints@whiterose.ac.uk
https://eprints.whiterose.ac.uk/

Materials Letters: X 7 (2020) 100052

Contents lists available at ScienceDirect

Materials Letters: X

journal homepage: www.elsevier.com/locate/mlblux

# Investigation of a novel AlZnN semiconductor alloy

A. Trapalis [a,*], P.W. Fry [a], K. Kennedy [b], I. Farrer [a], A. Kean [c], J. Sharman [c], J. Heffernan [a]

[a] Department of Electronic and Electrical Engineering, University of Sheffield, North Campus, Broad Lane, Sheffield S3 7HQ, United Kingdom
[b] Nanofabrication Core Lab, King Abdullah University of Science and Technology, Thuwal 23955-6900, Saudi Arabia
[c] Johnson Matthey, Blount's Court, RG4 9NH, United Kingdom

ARTICLE INFO

*Article history:*
Received 22 May 2020
Received in revised form 2 July 2020
Accepted 15 July 2020
Available online 20 July 2020

*Keywords:*
Physical vapour deposition
Semiconductors
Zinc nitride
Semiconductor alloy
Bandgap tuning

ABSTRACT

The formation of an AlZnN alloy was investigated as a route to tune the bandgap of $Zn_3N_2$. A significant shift of the bandgap was observed in the deposited films, increasing from 1.4 eV for $Zn_3N_2$ to 2.8 eV for AlZnN alloys with an AlN fraction of $\times$ = 0.19. The refractive index followed a similar trend, approaching that of AlN. The charge carrier density of AlZnN samples was significantly reduced reaching values in the order of $10^{16}$ $cm^{-3}$.

© 2020 The Author(s). Published by Elsevier B.V. This is an open access article under the CC BY license (http://creativecommons.org/licenses/by/4.0/).

## 1. Introduction

Zinc Nitride ($Zn_3N_2$) is a II-V semiconductor with potential for application in photonics devices, such as solar cells, because of its narrow direct bandgap and earth-abundant elemental composition [1–5]. The basic semiconductor properties of $Zn_3N_2$ have been demonstrated in simple devices such as thin-film transistors [6–9]. However, to meet the demands of advanced semiconductor applications such as heterojunction solar cells, a $Zn_3N_2$-compatible materials system must be developed that will allow bandgap engineering through semiconductor alloying, and the design of semiconductor heterostructures. The first investigation of such a materials system was reported by Wu et al., who demonstrated a $Mg_{3x}Zn_{3(1-x)}N_2$ semiconductor alloy with a tuneable bandgap in the range of 1.2–2.1 eV for Mg content up to $\times$ = 0.59 [10].

In this letter, we investigate the formation of an alternative AlZnN alloy and report the optical and electrical properties of such films. AlN is an interesting alloying candidate because it is already well established in the highly successful LED, laser and electronic technologies based on (Al)InGaN semiconductors. Furthermore, because of the wide bandgap of AlN, we anticipate that the bandgap of AlZnN will be tuneable over a wider range than that of MgZnN.

## 2. Experimental section

### 2.1. Film deposition

AlZnN films were deposited on unheated glass substrates by sputtering from an AlZn target (80 at. % Zn, 20 at. % Al) at a constant current of 400 mA in $N_2$ plasma. The base pressure in the deposition chamber was 7 $\times$ $10^{-7}$ Torr and the process pressure was in the order of $10^{-3}$ Torr. Sputtering in low $N_2$ flow rates (15 sccm) resulted in a low Al content in the deposited films, whilst higher Al concentration was obtained by sputtering in nitrogen-rich conditions (45 sccm). Under nitrogen-rich conditions, the different sputtering yields of Al and Zn species caused a gradual depletion of Zn from the surface of the target, resulting in the formation of films with higher Al content. Similar process parameters were used to deposit $Zn_3N_2$ using a Zn target in the same sputter chamber. The thickness of films studied here is in the range of 80 to 150 nm.

### 2.2. Characterisation

The physical, optical and electrical properties of the deposited films were studied by Energy Dispersive X-ray Spectroscopy (EDS), Grazing Incidence X-ray Diffraction (GIXRD) at 1° incidence, Spectroscopic Ellipsometry (SE) and Hall effect measurements, using the equipment detailed in previous papers [5,11]. For electrical measurements, ohmic contacts were obtained using high purity Indium annealed at 350 °C for 30 s.

* Corresponding author.
*E-mail address:* a.trapalis@sheffield.ac.uk (A. Trapalis).

https://doi.org/10.1016/j.mlblux.2020.100052
2590-1508/© 2020 The Author(s). Published by Elsevier B.V.
This is an open access article under the CC BY license (http://creativecommons.org/licenses/by/4.0/).

## 3. Results and discussion

The composition of the deposited films was evaluated with quantitative EDS analysis. The Zn and Al peaks of the EDS spectra are shown in Fig. 1a for 5 samples: ZN, a reference $Zn_3N_2$ sample, and AZN-1 to AZN-4, four AlZnN samples with increasing Al content. The samples were composed of Zn, Al, and N with the results listed in Table 1. Carbon and oxygen were also detected, however, in line with our previous experience of these materials, carbon is readily found as a surface contaminant (2–5 at. %), and oxygen is found in large amounts in the substrate, therefore they were deemed experimental artefacts and not a part of the film composition [5]. A binary alloy of the following form was considered: $Al_{2x}$-$Zn_{3(1-x)}N_2$. The AlN and $Zn_3N_2$ fractions were calculated from experimental Al, Zn, and N atomic fractions as:

$$x = \frac{Al}{\frac{2}{3}Zn + Al} \tag{1}$$

$$(1 - x) = \frac{2}{3}\frac{Zn}{N} \tag{2}$$

starting from the *Zn/Al* and *Zn/N* atomic ratios in $Al_{2x}Zn_{3(1-x)}N_2$. The calculated fractions are listed in Table 1 showing a maximum AlN fraction of × = 0.19 was obtained. The AlN and $Zn_3N_2$ fractions are plotted in Fig. 1b, demonstrating that the composition of AlZnN samples follows the expected trend of stoichiometric $Al_{2x}Zn_{3(1-x)}N_2$ (dashed line). It is likely that the deposited films have a N-rich composition because the average values for the two fractions are offset from the stoichiometric ratio and are in a N-rich region. Given this result, it is more accurate to refer to the composition as $Al_{2x}Zn_{3(1-x)}N_{2+}$<delta>.

The structure of the AlZnN films was investigated by GIXRD, shown in Fig. 1c. Diffraction peaks corresponding to crystal planes (400), (440), and (321) of the $Zn_3N_2$ structure were identified in the pattern of ZN [5,12]. These features shifted to higher angles in AZN samples, indicating that the size of the crystal lattice decreased as a result of the incorporation of Al into the structure. The preferred (400) orientation was strongly suppressed in samples AZN-2 and AZN-3 ($x$ > 0.10), and the additional observed diffraction peaks became broader as the films transitioned to an amorphous structure. We assign the broad features observed in AZN-2 and AZN-3 to the (321), (521), and (222) diffraction peaks, which are appropriately shifted from their expected positions in the $Zn_3N_2$ crystal structure because of Al incorporation. For instance, the diffraction peak (321) in AZN-2 is traced to its original position in sample ZN, shown by the dashed line in Fig. 1c. We attribute the transition to amorphous films to a non-optimal growth surface and growth conditions. However, the growth of single crystal AlZnN layers with high Al content may prove challenging even under optimised growth conditions because of the different crystal structures of $Zn_3N_2$ and cubic AlN.

The most direct evidence of alloying is the effect on the optical properties which we probe through SE measurements and by using a two-layer optical model consisting of: (a) the AlZnN film and (b) the glass substrate. The refractive index and extinction coefficient of the AlZnN samples obtained from the models are shown in Fig. 2a,b. For samples AZN-1 to AZN-4, there is a very clear shift of the absorption onset to higher energies, and the refractive index decreased accordingly. A Cody absorption plot was used to obtain the bandgap of each sample, shown in Fig. 2c [5,13]. The bandgap and refractive index obtained from this analysis are shown as a function of Al content in Fig. 3a,b. A shift of the optical properties of the AlZnN samples in the direction of AlN was observed with increasing Al content ($E_g$ = 5.34 eV and $n$ = 1.7 for cubic AlN) [14]. Note we refer to values for cubic AlN based on the principle that the structure of $Zn_3N_2$ is a cubic lattice and more likely to be compatible with cubic rather than the wurzite AlN structure. We report a maximum bandgap of 2.8 eV measured for × = 0.19.

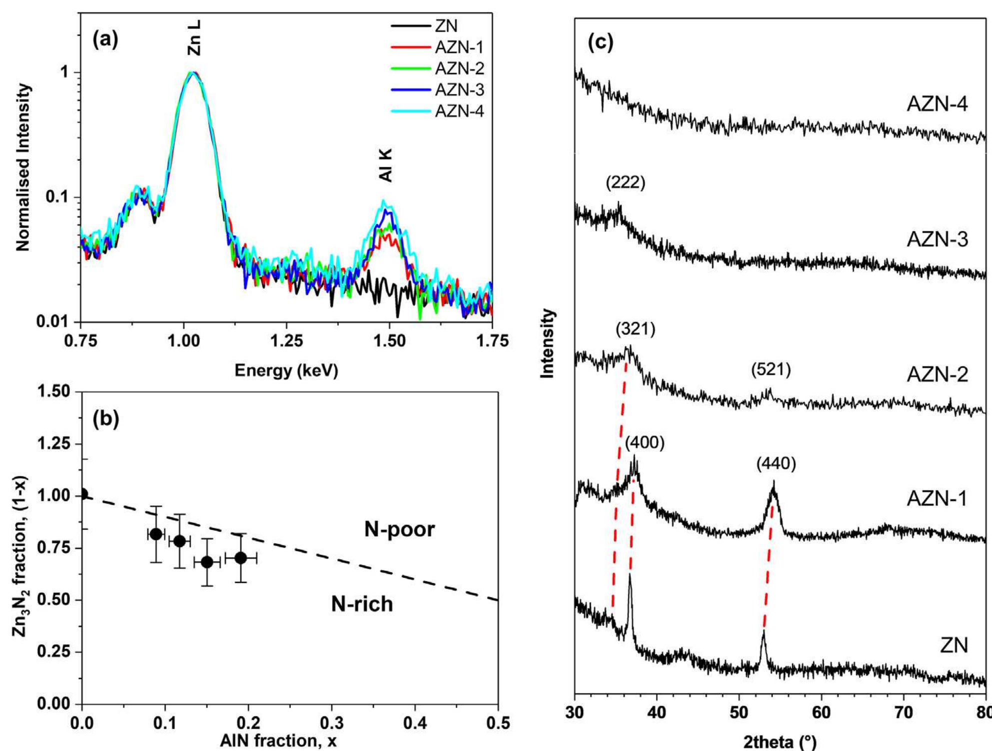


**Fig. 1.** (a) Zn and Al peaks in EDS spectra, (b) AlN fraction plotted against the $Zn_3N_2$ fraction, and (c) GIXRD measurements of samples ZN and AZN-1 to AZN-4. The dashed line in (b) indicates the stoichiometric ratio of $Al_{2x}Zn_{3(1-x)}N_2$.

**Table 1**
Compositional data for a $Zn_3N_2$ sample and different AlZnN samples obtained by quantitative EDS analysis.

| Sample | Zn (at. %) | Al (at. %) | N (at. %) | AlN fraction *x* | $Zn_3N_2$ fraction *(1-x)* |
|---|---|---|---|---|---|
| ZN | 60.3 | 0.0 | 39.7 | 0.00 | 1.01 ± 0.17 |
| AZN-1 | 53.1 | 3.5 | 43.4 | 0.09 ± 0.01 | 0.82 ± 0.14 |
| AZN-2 | 51.6 | 4.6 | 43.9 | 0.12 ± 0.01 | 0.78 ± 0.13 |
| AZN-3 | 47.7 | 5.6 | 46.6 | 0.15 ± 0.02 | 0.68 ± 0.11 |
| AZN-4 | 47.5 | 7.5 | 45.1 | 0.19 ± 0.02 | 0.70 ± 0.12 |

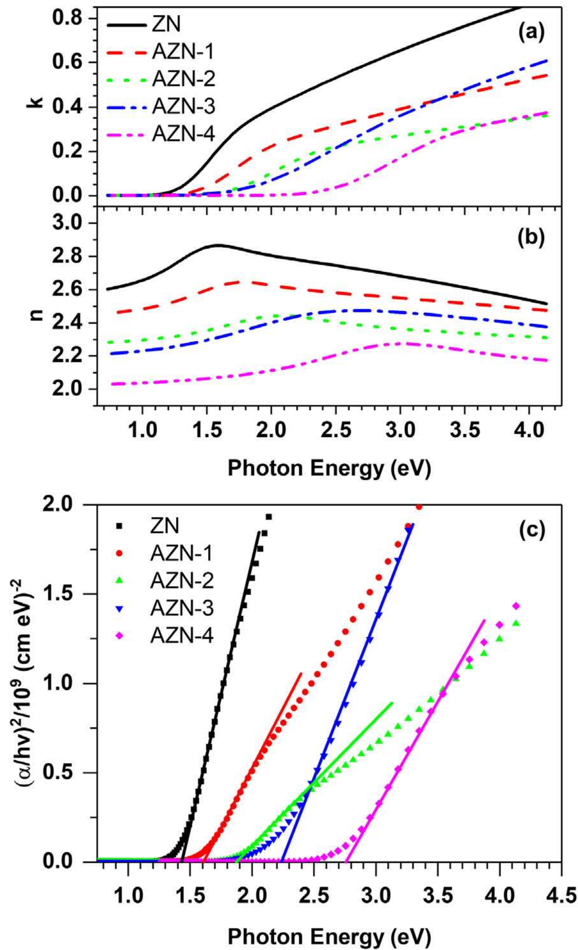


**Fig. 2.** (a) Extinction coefficient and (b) refractive index of AlZnN films obtained from ellipsometry measurements. (c) Cody plot analysis used to measure the optical bandgap of AlZnN films.

From Hall effect measurements, we obtained the resistivity and carrier density of the AlZnN samples, shown as a function of Al content in Fig. 3c, d. All measured samples displayed n-type conductivity as seen in $Zn_3N_2$ and also the recent demonstration of MgZnN. However, our AlZnN samples were found to have a significantly higher resistivity and lower carrier density than $Zn_3N_2$. The samples with the highest Al content could not be measured as they were effectively insulating, attributed to carrier depletion at the interfaces of the films which is observed in low-doped semiconductor thin films. The observation of a composition-dependent carrier density, which varies from $2 \times 10^{19}$ $cm^{-3}$ in $Zn_3N_2$ to less than $10^{17}$ $cm^{-3}$ in AZN-3 explains the non-linear dependence of the bandgap on composition seen in Fig. 3a. In the case of highly-doped $Zn_3N_2$ we expect a significant Burstein-Moss shift to increase the optical bandgap [3]. For the carrier densities measured in the AlZnN samples, the Burstein-Moss shift has little effect on the optical bandgap, and we can consider the measured bandgaps

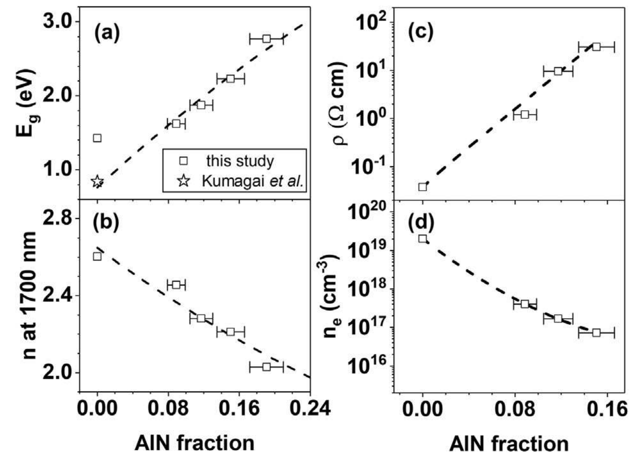


**Fig. 3.** (a) Optical bandgap, (b) refractive index, (c) resistivity, and (d) carrier concentration of different AlZnN films. The star (☆) in (a) shows the intrinsic bandgap of $Zn_3N_2$ as reported by Kumagai *et al.*[3] The dashed lines are intended as guides to the eye.

as intrinsic. A comprehensive first principles study by Kumagai *et al.* obtained a value of 0.84 eV for the intrinsic bandgap of $Zn_3N_2$ [3]. When this value is plotted in Fig. 3a, the bandgap dependence with Al content shows an approximately linear behaviour.

In $Zn_3N_2$ films, the unintentional n-type doping is often attributed to nitrogen vacancies and oxygen contamination [3,15]. We propose that the composition of the AlZnN samples studied here is introducing N-interstitials and Zn vacancies as compensating acceptor states [15]. Furthermore, we suggest that the binding energy of oxygen donor states may increase in AlZnN, as seen in oxygen-doped AlGaN [16]. The reduced carrier density of these samples is a promising result and suggests that further studies of AlZnN samples could provide insight on donor defects in $Zn_3N_2$. Furthermore, with a significant reduction in background n-type doping, these results suggest that high-quality AlZnN samples are candidates to realise p-type doping in this materials system.

## 4. Conclusions

In summary, we have investigated the optical and electrical properties of AlZnN alloys with a maximum AlN fraction of $\times$ = 0.19. Analysis of optical measurements showed that the deposited films were semiconductor alloys with properties between $Zn_3N_2$ and AlN. A maximum bandgap of 2.8 eV was measured for $\times$ = 0.19. The electrical properties of the AlZnN films changed drastically, reaching carrier concentrations as low as $7x10^{16}$ $cm^{-3}$, which was attributed to partial compensation and potentially an increase in the donor binding energy with increasing Al content. This low intrinsic doping suggests that high-quality AlZnN is a good candidate for the development of p-type doping in $Zn_3N_2$-related materials, which is a critical step to demonstrating devices such as lasers, LEDs and solar cells. These results all point to AlZnN being an attractive alloy system for use in heterostructures based on $Zn_3N_2$.

## Declaration of Competing Interest

The authors declare that they have no known competing financial interests or personal relationships that could have appeared to influence the work reported in this paper.

## Acknowledgements

The authors wish to acknowledge funding by the EPSRC (Engineering and Physical Science Research Council, EP/M507611/1) the two funders contributed to the same grant ID in an Industrial CASE Award and Johnson Matthey PLC (Award No. 14550005). The data presented in this paper is available to download for free with the following DOI: 10.15131/shef.data.12327560.

## Appendix A. Supplementary data

Supplementary data to this article can be found online at https://doi.org/10.1016/j.mlblux.2020.100052.

## References

[1] C.G. Núñez, J.L. Pau, M.J. Hernández, M. Cervera, J. Piqueras, Appl. Phys. Lett. 99 (2011) 232112.
[2] M. Ullah, G. Murtaza, M. Yaseen, S.A. Khan, J. Alloy. Compd. (2017).
[3] Y. Kumagai, K. Harada, H. Akamatsu, K. Matsuzaki, F. Oba, Phys. Rev. Appl 8 (2017) 014015.
[4] A. Trapalis, I. Farrer, K. Kennedy, A. Kean, J. Sharman, J. Heffernan, Appl. Phys. Lett. 111 (2017) 122105.
[5] A. Trapalis, J. Heffernan, I. Farrer, J. Sharman, A. Kean, J. Appl. Phys. 120 (2016) 205102.
[6] C.G. Núñez, J.L. Pau, E. Ruiz, J. Piqueras, Appl. Phys. Lett. 101 (2012) 253501.
[7] S.R. Bhattacharyya, R. Ayouchi, M. Pinnisch, R. Schwarz, Physica Status Solidi (c) 9 (2012) 469.
[8] S. Sinha, D. Choudhury, G. Rajaraman, S.K. Sarkar, RSC Adv. 5 (2015) 22712.
[9] M.A. Dominguez, J.L. Pau, M. Gómez-Castaño, J.A. Luna-Lopez, P. Rosales, Thin Solid Films 619 (2016) 261.
[10] P. Wu, X. Cao, T. Tiedje, N. Yamada, Mater. Lett. 236 (2019) 649.
[11] A. Trapalis, I. Farrer, K. Kennedy, A. Kean, J. Sharman, J. Heffernan, AIP Adv. 10 (2020) 035018.
[12] T. Suda, K. Kakishita, J. Appl. Phys. 99 (2006) 076101.
[13] M.E. Sánchez-Vergara, J.C. Alonso-Huitron, A. Rodriguez-Gómez, J.N. Reider-Burstin, Molecules 17 (2012) 10000.
[14] M.P. Thompson, G.W. Auner, T.S. Zheleva, K.A. Jones, S.J. Simko, J.N. Hilfiker, Journal of Applied Physics 89 (2001) 3331.
[15] N. Jiang, J.L. Roehl, S.V. Khare, D.G. Georgiev, A.H. Jayatissa, Thin Solid Films 564 (2014) 331.
[16] M.D. McCluskey, N.M. Johnson, C.G. Van de Walle, D.P. Bour, M. Kneissl, W. Walukiewicz, Phys. Rev. Lett. 80 (1998) 4008.